Goure-Doubi et al., J Material Sci Eng 2018, 7:1
DOI: 10.4172/2169-0022.1000409

Journal of Material Sciences & Engineering

Research Article Open Access

^{29}Si and ^{27}Al MAS NMR Characterization of the Structural Evolution of a Lateritic Clay under Acidic and Alkaline Treatments

Herve Goure-Doubi[1], Valérie Montouillout[2], Gisèle L Lecomte-Nana[1]*, Benoît Naît-Ali[1], Léon Koffi Konan[3] and Agnès Smith[1]

[1]*GEMH - Groupe d'Etude des Matériaux Hétérogènes, 12 rue Atlantis, 87068 Limoges Cedex, France*
[2]*CEMHTI - Conditions Extrêmes et Matériaux: Haute Température et Irradiation, UPR3079 CNRS, 7 1D avenue de la Recherche Scientifique, 45071 Orléans cedex 2, France*
[3]*LCMI - Laboratory of Inorganic Materials Chemistry, Félix Houphouët-Boigny University, 22 BP 582 Abidjan 22, Ivory Coast*

Abstract

In the present work the modifications induced by the geomimetic processing on the environment of silicon and aluminum atoms are finely characterized by solid state MAS NMR. The raw clay (Lat), a lateritic clay from Yaoundé (Cameroon), contains kaolinite, quartz, hematite and goethite as major mineral phases. This material is treated under acidic conditions during 24 h (LatAF) and then under alkaline conditions during 18 days, leading to the final consolidated "geomimetic" product (LatAFCH). The samples have been characterized by ^{29}Si and ^{27}Al solid state NMR at each step of the process.

The NMR spectra obtained for the starting clay indicate the presence of Al_{IV} and Al_{VI} populations together with silicon Q^2(0 or 1Al) and Q^3(0 or 1Al) environments located at δ_{iso}=-83 ppm and δ_{iso}=-91 ppm respectively.

The acidic reaction during 24 h, does not significantly affect the silicon-rich layers. It induces a conversion of part of Al_{IV} population into Al_{VI} environment mainly related to the occurrence of six-fold organo-aluminum complexes when using fulvic acid. With inorganic acid, Al dissolution prevails.

The neutralization (using lime) of the medium, followed by ageing for 18 days, promotes clay interactions with available calcium ions. The newly formed phases are cementitious CSH, CASH and CAH phases.

Keywords: MAS NMR; Lateritic clay; Kaolinite; Fulvic acid; Alkaline; Geomimetic material

Introduction

Clays are natural raw materials characterized by a layered structure and therefore belonging to the phyllosilicate family. There are two groups of phyllosilicates depending on the constitution of an elementary sheet resulting from a pilling up of octahedral (Al and/or Mg cations) and tetrahedral (Si cations) layers along the c-axis [1-4]: 1:1 or Te-Oc phyllosilicate group that exhibits an octahedral layer combined to a tetrahedral layer, typically as in kaolinite where the characteristic d-spacing of the elementary sheet is 0.714 nm and the 2:1 phyllosilicate group characterized by an elementary sheet composed of one octahedral layer sandwiched between two tetrahedral layers to form an elementary sheet. Due to the occurrence of various cation substitutions within the octahedral and/or tetrahedral layers, the global sheet is often negatively charged and balanced by compensating cations present within the interlayer space [4-8]. The d-spacing is in the range of 0.9 to 1.4 nm in general and typical clay minerals of this group are montmorillonites, vermiculites, talc, illite, mica …

These raw materials are readily available and can be easily recycled, they are therefore involved in sustainable and environmentally friendly applications. Clays commonly include, together with clay minerals, various amounts of associated phases or secondary phases such as quartz, feldspar, iron oxides or oxy-hydroxides, carbonates as well as titanium oxides. In tropical regions [9-15], the major type of associated phase is iron oxide and/or oxy-hydroxide. These associated iron phases are responsible for the yellowish-reddish to dark-brown colors of related clays. In literature, clay is considered as lateritic clay when the amount of iron phases is in the range of 15-25 mass% in association with near to 50% mass clay minerals. Such raw materials are mainly used for road and building purposes. The consolidation of lateritic clay products is generally performed through firing, compaction or stabilization using hydraulic binders (cements, lime). However, a processing including acidic and alkaline consolidating reactions to obtain "geomimetic" materials has recently been proposed [16]. Different characterization (XRD and DTA-TGA) were carried out on these geomimetics materials products to understand the strengthening mechanisms during the key processing steps [6,17,18]. Results clearly indicate the occurrence of new crystalline phases that may result from dissolution-precipitation mechanisms during the 24 h acidic reaction followed by alkaline neutralization and ageing at 60°C for 18 days under saturated water atmosphere. There are still some misunderstands regarding the potential occurrence of amorphous binding phases. The present work is aiming to contribute to clear up the latter point by the investigation of the evolution of the local environment of the main constitutive atoms namely Si and Al using solid state MAS NMR analyses.

Materials and Methods

The raw clay (labeled as Lat) is a lateritic clay from Yaoundé town (Cameroon, Awae deposit, South-east of Yaoundé, 3°49" to 3°51" North latitude and 11°33" to 11°35" East longitude). It is naturally rich in iron compounds. A KGa-2 kaolin (labeled K) from the clay mineralogy society in Georgia is also used in this work. This reference

***Corresponding author:** Gisèle L Lecomte-Nana, GEMH: Groupe d'Etude des Matériaux Hétérogènes, Centre Européen de la Céramique – GEMH, 12 rue Atlantis, 87068 Limoges Cedex, France, Tel: +33 (0) 587 50 25 59; Fax: +33 (0) 587 50 23 01; E-mail: gisele.lecomte@unilim.fr

Received November 22, 2017; **Accepted** December 26 , 2017; **Published** January 03, 2018

Citation: Goure-Doubi H, Montouillout V, Lecomte-Nana GL, Naît-Ali B, Koffi Konan L, et al. (2018) Effect of Durable Superhydrophobic FS/PS Using DCTES on Carbon Steel. J Material Sci Eng 7: 409. doi: 10.4172/2169-0022.1000409

kaolin contains a poorly-crystalline kaolinite as in the raw lateritic clay (similar crystallinity, R2 index).

Additional reagents are fulvic acid (an organic macromolecule having several functional groups Figure 1 [19] purchased from Bois Valor in France and lime (99.9 mass% of $Ca(OH)_2$) provided by Aldrich.

Chemical analysis

The chemical composition of clays was determined using Inductively Coupled Plasma Atomic Emission Spectrometry (ICP-AES). Prior to analysis, dried sample powders were dissolved using microwaves under acidic (hydrofluoric and nitric acids) and high pressure conditions. A CEM MARS 5 microwave was used and the dissolution was achieved after a 45 min cycle including a maximum temperature and pressure of 180°C and 3 MPa, respectively.

X-ray diffraction (XRD)

X-ray diffraction (XRD) analyses were conducted on powdered samples with a Bruker-AXS D5000 powder diffractometer using $K\alpha_1$ radiation of Cu and a graphite back-monochromator. XRD experiments have been achieved in step-scan mode from 3° to 45° (2θ) with a counting time of 10.1 s per 0.02° step. Crystalline phases were identified by comparison with PDF standards (Powder Diffraction Files) from ICDD (the International Center for Diffraction Data).

Thermal analysis (DTA-TGA)

Differential thermal and thermogravimetric analyses (DTA and TGA) were carried out between 25°C and 1200°C at 5°C/min under dried-air atmosphere using SETSYS Evolution DTA-TGA equipment from SETARAM. The samples were previously crushed and sieved at 100 µm, then oven-dried at 40°C for at least one week or until the achievement of no mass variation. Alumina powder, previously heated at 1500°C for one hour, was used as a reference material. All analyses were performed using 60 mg aliquots of sample and reference.

Scanning electron microscopy (SEM) and Specific surface area measurements

The observation of some samples microstructure have been performed by scanning electron microscopy (SEM) using a Stereoscan 260 apparatus equipped with a PGT Prism energy dispersive spectrometry analyzer. Prior to their observation, the samples were dried at 60°C for one week and metallization was conducted through the sputtering of a nanometric layer of platinum onto the sample surface.

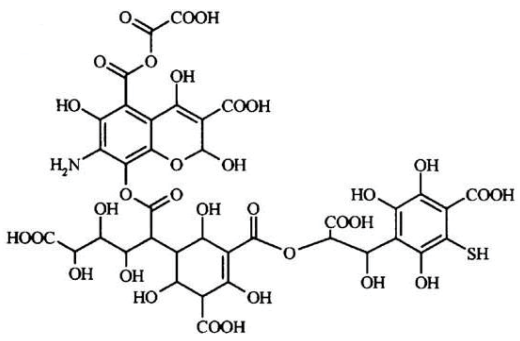

Figure 1: Basic structural model of a fulvic acid proposed by Alvarez-Puebla et al. [19].

The Brunauer Emmet and Teller method was used to determine the specific surface area of the samples, using TriStar II equipment from Micromeritics. Measurements were carried out after a 16 hours degassing step at 150°C, on dried samples previously crushed and sieved to 100 µm.

Solid state magic angle spinning nuclear magnetic resonance (SSMAS NMR)

High-resolution ^{29}Si MAS NMR spectra were acquired at room temperature on a Bruker 400 spectrometer operating at a Larmor frequency of 79.5 MHz and using a spinning rate of 10 kHz. Each spectrum necessitated the sum of 10000 to 20000 transients accumulated with a recycling delay of 10 s insuring complete relaxation of the magnetization.

^{27}Al MAS NMR experiments were conducted on an AVANCE 750 spectrometer operating at 195 MHz with very high MAS conditions (spinning rate of 60 kHz). The spectra were acquired after a single short pulse (π/12) ensuring a quantitative excitation and quantification of ^{27}Al central transition. The recycling delay was fixed at 1 s.

The chemical shift were referenced relative to TMS and $Al(NO_3)_3$ 1 M solution for ^{29}Si and ^{27}Al respectively. Quantitative analyses of the ^{29}Si and ^{27}Al MAS NMR spectra were performed with the Dmfit program [20].

In the spectra interpretation, we used the Q^n notation, commonly used to describe the structure of silicate anions: Q represents a silicon atom bonded to four oxygen atoms, forming a SiO_4 tetrahedron; the superscript n indicates the connectivity, i.e., the number of other Q units attached to the SiO_4 tetrahedron. Q^0 denotes the monomeric orthosilicate anion $(SiO_4)^{4-}$, Q^1 represents the end groups of chains, while Q^2, Q^3, and Q^4 are used respectively for the middle groups of chains or cycles, groups at chain-branching sites, and three-dimensionally cross-linked groups. Dealing with alumino-silicates, some of the neighboring Si atoms in the tetrahedral layer could be Al. In this case, the number of AlO_4 tetrahedral bound to the central silicon of a Q^n unit is given in parentheses; namely, $Q^n(m\text{Al})$ indicates a SiO_4 group connected to mAl and $(n - m)$ other Si atoms via oxygen bridges, where n is in the range 0 to 4 and $m \leq n$.

The processing of geomimetic materials (Figure 2) was described in previous papers [6,18]. Prior to elaboration, the raw clay (Lat sample) was ground and sieved under 100 micrometers. The acidic solutions were prepared by a homogeneous mixing during 5 min of fulvic acid (V_{AF}) and deionized water (V_W) to obtain a final pH value of 2. This acid solution was noted AF. The Lat sample was then added and mixed with AF for 24 h. Finally, lime, noted CH, was added and the mixture is left to cure at 60°C for 18 days. The solid part, S, consists of 80 mass% of Lat clay (Lat) and 20 mass% of lime (CH). The quantities were calculated in order to obtain a final mass ratio, water over solid, equal to 0.29. After 24 h of reaction with acid, the sample was labeled as LatAF. The final consolidated "geomimetic" material was labeled as LatAFCH.

Results and Discussion

Mineralogical and structural characterization

The chemical and mineralogical compositions of this lateritic clay (Lat) (Table 1) indicate the presence of aluminum, silicon, and iron oxides as major constituents. The density and BET surface area of the starting powder are 2.8 g/cm^3 and 48 m^2/g respectively. The particles are stacked together and appear as aggregates with a mean size of 1 µm [6]. Such high specific surface area may arise from the presence of iron

phase nodules onto the surface of clay platelets as well as from the high alteration (natural leaching) of this type of lateritic soil.

The X-ray diffraction patterns obtained for Lat and LatAFCH are shown on Figure 3. Kaolinite, goethite, hematite and quartz are present in both the raw clay (Lat) and the consolidated material (LatAFCH). However, two new phases were detected for LatAFCH: the katoite ($Ca_3Al_2(SiO_2)(OH)_8$), a cementitous phase, i.e calcium aluminum silicate hydrate (noted CASH, where C, A, S and H stand respectively for CaO, Al_2O_3, SiO_2 and H_2O), and the richterite ($K_{0.9}Na_{1.6}Ca_{0.5}Fe_5Si_8O_{22}(OH)_2$), an hydroxylated phase containing silicon, iron, sodium, potassium and calcium. The presence of katoite suggests that during the consolidation process, siliceous and aluminous ions contained in the lateritic clay would dissolve and re-precipitate in the form of hydrated cementitous phases such as CASH, CAH or amorphous CSH [21]. The formation of richterite appears to be the result of dissolution and precipitation reactions involving iron compounds and clay platelets.

Thermal analysis of the different materials gives complementary information about the nature of the mineral phases present in the starting lateritic clay or in the consolidated clays. The thermal transformations occurring during the heat treatment of the starting lateritic clay and the resulting "geomimetic" materials are shown in Figure 4. These DTA-TGA curves exhibit many differences. In the 100-200°C range, the endothermic peak might be related to the departure of physisorbed water. This peak is associated with a mass loss of 1.05% for the lateritic clay (Lat) and with a mass loss of 2.2% for the consolidated material (LatAFCH). The increase of the mass loss and also the temperature range could be the signature of the thermal decomposition of CSH phases [21].

In the 200-400°C range, while the lateritic clay shows an endothermic phenomenon, the "geomimetic" material presents an exothermic peak. This phenomenon can be due to the organic matter decomposition, to the transformation of ferrihydrite into hematite or to the oxidation of organic matter [22,23].

In the 900-1000°C range, the exothermic peak, characteristic of structural reorganization in the lateritic clay is significantly reduced in the case of the consolidated material (LatAFCH). This observation can be explained by the diffusion of iron, from iron nodules present on the surface of kaolinite platelets, into the metakaolinite network, affecting the structural reorganization [24].

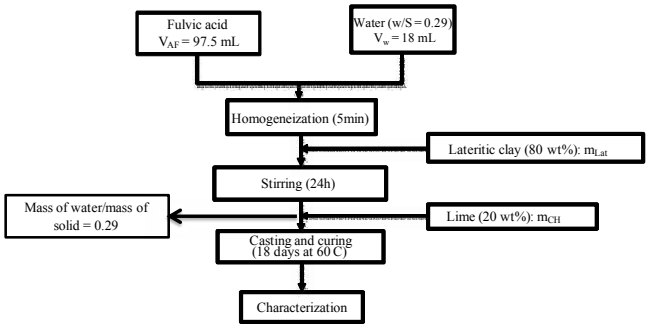

Figure 2: Flowchart of the elaboration process of "geomimetic" materials [16]. m_{Lat} and m_{CH} correspond to the mass of lateric clay and lime respectively.

	SiO_2	Al_2O_3	Fe_2O_3	CaO	MgO	Na_2O	K_2O	TiO_2
Chemical Composition (%)	46.18	27.2	23.41	1.04	0.02	0.24	0.2	1.84
Mineralogical Composition (%)	Kaolinite=55.1; Quartz=21.2; Goethite=21.3; Hematite=2.4; Ferrihydrite (traces)							

Table 1: Chemical and mineralogical compositions (mass%) of raw lateritic clay.

Solid state MAS NMR characterization

To allow a better understanding of the structural evolution of materials after acidic and alkaline treatment, a systematic ^{27}Al and ^{29}Si NMR analyses was performed on four series of samples. The first series was composed of the Lat, LatAF and LatAFCH samples studied so far. The second series was based on a KGa-2 reference kaolin that was subjected to the same treatment (KGa-2, KGa-2AF, and KGa-2AFCH samples) and finally the third and fourth series were obtained from the same Lateritic and KGa-2 reference kaolin, treated in the first step using nitric acid (HNO_3), the second step remaining unchanged (Lat, LatAN, LatANCH and KGa-2, KGa-2AN, KGa-2ANCH samples). ^{27}Al and ^{29}Si MAS NMR spectra are shown on Figures 5 and 6 respectively.

The ^{27}Al MAS spectrum of the raw clay, Lat sample, exhibits two symmetric signals centered at 70.6 ppm and 5.7 ppm assigned to 4-fold coordinated (Al_{IV}) and 6-fold coordinated aluminum [25] respectively (Figure 5A). Despite the quadrupolar nature of ^{27}Al (I=5/2), both signals appear narrow (FWHM are 1.2 and 1.1 kHz respectively), symmetric and can be unambiguously simulated using Gaussian line shape. Taken into ccount that the spectrum was acquired at quite a high magnetic field (17.6 Tesla), the observed line shapes indicate a relatively symmetric environment for aluminum characterized by a low electric field gradient, and then a very low quadrupolar interaction.

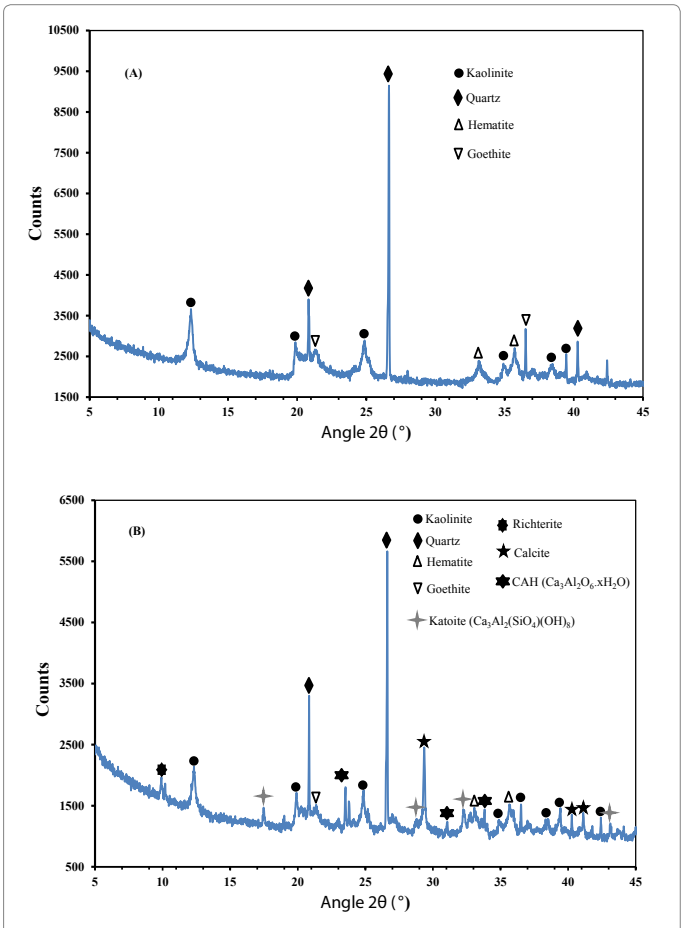

Figure 3: XRD diagram of (A) the lateritic clay and (B) the "geomimetic" material.

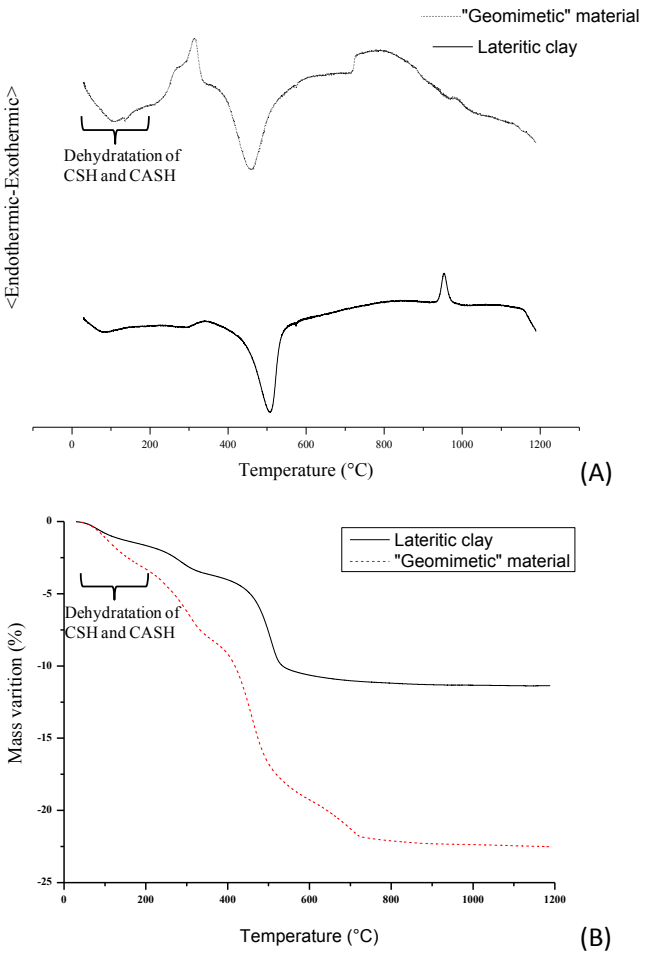

Figure 4: Differential thermal analysis (**A**) and thermogravimetric (B) of the lateritic clay and "geomimetic" material.

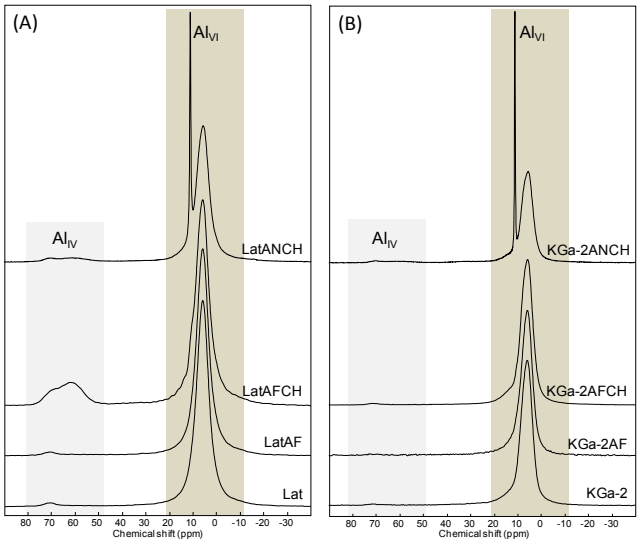

Figure 5: ^{27}Al MAS NMR spectra of (A) lateritic clay and (B) KGa-2 series.

The deconvolution of the spectrum leads to the estimation of Al_{IV} and Al_{VI} species to 3% and 97% respectively, consistent with the presence of small fraction of a 2:1 clay mineral together with the major 1:1 clay mineral phase (kaolinite) [26-31] detected on XRD diagram (Figure 3A). The 2:1 clay mineral has not been identified by XRD, probably due to a content less than 5 mass%. It should be noted, that the observed ^{27}Al NMR signals does not seem affected by the presence the high iron content (23.4 mass% of Fe_2O_3), neither signal broadening nor very short relaxation times can be observed. This was explained by the location of iron which is essentially in goethite, hematite and ferrihydrite phases and then by a very low iron substitution in clay mineral phases. However, we cannot completely exclude that a slight part of aluminum signal is unobservable, due to paramagnetic interaction with substituted iron cations.

The ^{27}Al NMR spectrum (Figure 5A) of the sample treated under acidic conditions (LatAF) is quite completely equivalent, except a slight increase of the Al_{VI}/Al_{IV} ratio. At this stage, it is difficult to distinguish whether the Al environment has been highly modified. Interestingly, the treatment under alkaline conditions induces more distinguishable differences on aluminum environment. The ^{27}Al spectrum of LAFCH exhibits additional signals, both in the Al_{IV} and in the Al_{VI} chemical shift ranges. Without going more ahead in details, aluminum is now at 18% four-fold coordinated and 82% six-fold coordinated. This observation, together with the results of XRD and DTA-TGA analyses, translates a strong interaction between alkaline cations and the Al provided by Lat. ^{29}Si MAS NMR spectra of the raw clay (Lat), LatAF and LatAFCH are shown in Figure 6A. The Lat and LatAF spectra are completely equivalent, composed of two distinguishable narrow peaks centered at -83 ppm (FWHM=200 Hz), and -91 ppm (FWHM=300 Hz). The signal at -83 ppm can be attributed to Q^2(1Al), and Q^2(0Al) while the signal at -91 ppm may correspond to Q^3(1Al) or Q^3(0Al). These results are in agreement with the presence of kaolinite as expected in lateritic clay. Furthermore, the Q^2(1Al) and Q^3(1Al) environments are consistent with the presence of 2:1 clay mineral as also noted regarding the Al_{IV} detected on the ^{27}Al NMR spectrum (Figure 5A) of Lat sample. The Q^2(1Al),environments are characteristic of Si-contained units at the edges of clay minerals. The spectrum of the final "geomimetic" product, LatAFCH, seems also quite similar. However, we can distinguish the presence of an additional narrow signal centered at -86

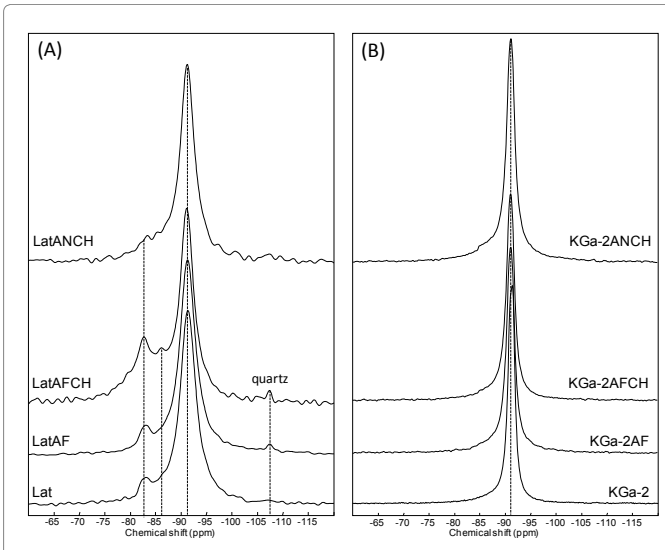

Figure 6: ^{29}Si MAS NMR spectra of (A) lateritic clay and (B) Kga-2 series.

ppm (FWHM=200Hz) but also a large contribution under the main resonances. The slight signal can be assigned to a Q^2(1Al) environment of silicon atoms and the large contribution could probably be related to the new Al_{IV} species observed on ^{27}Al spectrum of LatAFCH. The substitution of aluminum in the silicate layer induce the existence of Qn(mAl) species and then the overlapping of numerous ^{29}Si signal. This is in agreement with the formation of new binding silicate phases during the strengthening of the "geomimetic" products.

Two additional remarks: first we observed on LatAF and LatAFCH spectra, the presence of a very small signal at -107 ppm. This signal could be related to the quartz phase detected by XRD. Its amount is then certainly under-estimated on NMR analysis due to the spectral acquisition conditions (recycling delay too short to ensure complete relaxation of this specific signal). The second remark concerns the effect of iron presence. As for aluminum, the spectra do not show any paramagnetic effect, however it cannot be excluded that part of the signal is undetectable. ^{27}Al and ^{29}Si high resolution MAS NMR spectra obtained on the raw kaolin (KGa-2) and upon subsequent reactions (KGa-2AF and KGa-2AFCH), as described with the Lat sample, are shown in Figures 5B and 6B respectively. ^{27}Al spectrum exhibits a main signal centered at 5.9 ppm corresponding to six-fold aluminum species, and a slight signal, corresponding to less than 1% of the total intensity, is detected in the chemical range of four-fold aluminum. ^{29}Si spectrum is very simple, constituted of only one narrow signal centered at -91 ppm (FWHM=123 Hz) corresponding to Q^3(0 or 1Al). As for lateritic clay, the environment of aluminum and silicon do not seem affected by the acidic treatment: ^{27}Al and ^{29}Si spectra of KGa-2 and KGa-2AF are similar. After the alkaline treatment, the ^{29}Si environment remains unaffected (no new signal is detected), and the ^{27}Al spectrum of KGa-2AFCH exhibits only a new shoulder on the left side of the main signal corresponding to additional Al_{VI} species. The structural evolution of KGa-2 is minimal under these conditions.

Finally in the case of the series which have undergone the same process but with nitric acid, no modification is observed on ^{27}Al and ^{29}Si spectra after the first step (not shown) either for lateritic clay or KGa-2 reference kaolin. On the contrary, some differences are noticed on the consolidated products, LatANCH and KGa-2ANCH ^{27}Al spectra (Figures 5B and 6B). For both of them, we observed a new sharp resonance (δ_{iso}=11 ppm, FWHM=80 Hz) indicating the presence of a new 6-fold Al species. This species was not detected in the sample treated with the fulvic acid. Considering XRD characterization, this signal can be attributed to the highly soluble calcium aluminum nitrate. The XRD diffraction of the material LatANCH shows (Figure 7) the presence of the phases detected in the starting clay namely: kaolinite, goethite, hematite and quartz. In addition, a new phase appears in the material LatANCH and is identified as a hydrated calcium aluminum nitrate ($Ca_6Al_2O_6(NO_3)_6.xH_2O$). This newly formed nitrate belongs to the family of compounds called layered double hydroxides of aluminum and calcium. Its crystalline structure is typical of that of a calcium sulfoaluminate type phase (noted AFm). Moreover, in the case of LatANCH sample, we observe the same new Al_{IV} signal as in the case of LatAFCH in a smaller quantity (the final Al_{VI}/Al_{IV} ratio are ~15 and ~4 respectively). No new Al_{iv} species are detected for KGa-2ANCH. In parallel, the ^{29}Si spectrum of LatANCH consolidated product exhibits the same large contribution and the additional narrow signal centered at -86 ppm as observed for LatAFCH, once again in lower quantities. These signals are not present on KGa-2ANCH spectrum. These observations confirm our assumption that these silicon species belong to the same phase than the new tetrahedral aluminum species.

These results seem to indicate on the one hand that the inorganic acid is more aggressive with the lateritic clay than the organic acid, which tends to form organic-mineral complexes [32], and in the other hand that the lateritic clay is more reactive that the KGa-2 kaolin.

Summarized considerations

The acidic reaction seems to have a minor influence on lateritic clay structure. The NMR results indicate only a low difference in the Al_{VI}/Al_{IV} ratio, and no observable difference on silicon environment. Some ICP – AES analysis of the filtrate recovered after 24 h reaction of Lat with fulvic acid indicate that together with iron, 0.62 mass% of initial Al_2O_3 is dissolved during this acidic attack. One can then imagine that in our "geomimetic" process the 2:1 clay mineral (where aluminum occurs in tetrahedral environment) is partially dissolved and re-precipitate forming an Al-fulvic acid complexes in which aluminum atoms are now six-fold coordinated. This dissolution-reaction is unfortunately too scarce to induce the formation of a new distinguishable Al_{VI} site, but is coherent with the increase of the Al_{VI}/Al_{IV} ratio.

On the contrary, the alkaline neutralization and curing at 60°C for 18 days under saturated water atmosphere induced a strong modification of the lateritic clay. NMR results on LatAFCH sample indicate a significant modification of both Al and Si environment. The occurrence of new Al_{IV} sites indicates the formation new Al-containing phases, as probably the expected amorphous hydrated calcium aluminum silicate (C-A-S-H), similar to cementitious binding phases. The katoite identified by XRD characterization of the LatAFCH contains tetrahedrally coordinated as well as octahedrally coordinated aluminum. According to literature [33,34], unhydrated katoite contains mainly Al_{IV} sites while hydrated and partially Si-substituted katoite exhibits mainly Al_{VI} sites located at 12.4 ppm and 5.3 ppm. Our "geomimetic" sample seems to contain a hydrated Si-containing katoite. The presence of the ^{29}Si peak at -86 ppm is in agreement with a concomitant formation of pure hydrated calcium silicate (CSH) gels [35,36] as suggested from DTA-TGA thermograms (Figure 5).

It can therefore be assumed that the governing reactions during the acidic stage are summarized by eqns. (1)-(3) (R stands for the organic part of the macromolecule). In fact, with organic acid, a six-fold organic-aluminum complex is formed.

$$Si_2Al_2O_5(OH)_4 + 6H^+ \rightarrow 2H_4SiO_4 + 2Al^{3+} + H_2O \quad (1)$$

$$RCOOH \rightarrow RCOO^- + H^+ \quad (2)$$

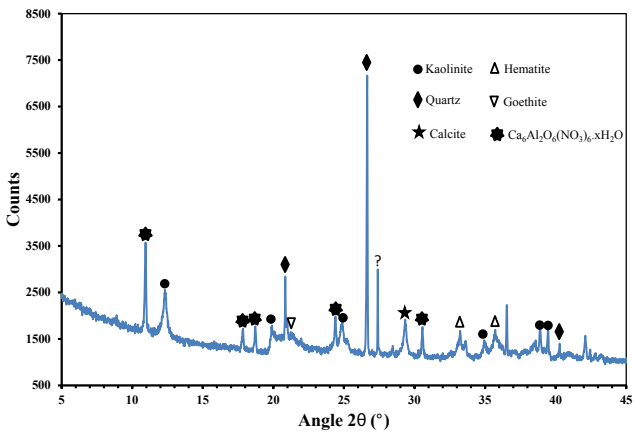

Figure 7: XRD diagram of the material LatANCH.

$$K_{aolinite} + RCOO^{-} + H^{+} \rightarrow AlOOCR \quad (3)$$

After the alkaline neutralization (pH > 11), the 18 days of ageing enhances subsequent reactions leading to the consolidated products. These reactions, involves both silicon and aluminum environments modifications. Considering a given clay mineral, the various reactions are described through eqns. (4)-(8). Partially solubilized silicon-rich and aluminium –rich layers are combining to available calcium cations to form the different cementitious CSH, CASH and CAH like phases. The stoichiometry of these species can vary depending on the ageing period. Nevertheless, the involved reaction kinetic is too slow at room temperature and the detected phases after the optimized strengthening can be considered stable upon a year.

$$Ca(OH)_2 \rightarrow Ca^{2+} + +2(OH)^{-} \quad (4)$$

$$Si_2Al_2O_5(OH)_4 + 2(OH)^{-} + 5H_2O \rightarrow 2Al(OH)_4^{-} + 2H_4SiO_4 \quad (5)$$

$$H_2SiO_4 \rightarrow H_3SiO_4^{-} + H^{+} \rightarrow H_2SiO_4^{2+} + 2H^{+} \quad (6)$$

$$3Ca^{2+} + 2Al(OH)_4^{-} + 4(OH)^{-} \rightarrow Ca_3Al_2(OH)_{12} \Leftrightarrow 3CaO.Al_2O_3.6H_2O(C_3AH_6) \quad (7)$$

$$Ca^{2+} + H_2SiO_4^{-} \rightarrow CaH_2SiO_4 \Leftrightarrow CaO.SiO_2.H_2O(\text{CSHgel}) \quad (8)$$

Conclusion

"Geomimetic" materials, obtained using raw lateritic clay, under acidic and alkaline treatments have been finely characterized using ^{29}Si and ^{27}Al solid state MAS NMR.

Both Al_{IV} and Al_{VI} species have been evidenced in the raw clay (Lat). The acidic reaction seems to lead to the conversion of a fraction of the four-fold coordinated aluminum into six-fold coordinated aluminum, in agreement with a dissolution-precipitation reaction. The alkaline condition tends to increase the later reaction since new Al_{IV} and Al_{VI} species appear at 61.6 ppm and 12.5 ppm respectively.

The silicon atoms within the Lat clay are related to $Q^2(0Al)$ or $Q^2(1Al)$ located at δ_{iso}=-83

ppm, and to $Q^3(0Al)$ and $Q^3(1Al)$ environments located at δ_{iso}=-91 and -90 ppm. The enlargement of $Q^3(0Al)$ peak at the expense of the for the former peaks located at δ_{iso}=-83 ppm (Q^2 or Q^3) noted for LatAF, was consistent with an amorphization of the initial clay minerals. A new peak is observed at -86 ppm and is assigned to a $Q^2(1Al)$ environment within LatAFCH. The latter indicates a greater alteration and redistribution of silicon atoms under alkaline conditions together with curing.

The observed trends together with XRD and DTA-TGA characterizations allow to comfort the assumption of the occurrence of consolidating crystalline (katoite and richterite) and cementitious gel-like CSH (hydrated calcium silicate), CSAH (hydrated calcium and aluminum silicate) and CAH (hydrated calcium aluminate) phases. Furthermore, it appears that the use of fulvic acid partially inhibits the alkaline interaction and promotes the formation of aluminum hydroxide phase that might be responsible of the surface aspect observed with as-obtained "geomimetic" products.

Acknowledgements

Financial support from the TGIR-RMN-THC Fr3050 CNRS for conducting the research is gratefully acknowledged. We would like to thank Prof. Dominique MASSIOT for guiding us during this study.

References

1. Billault V, Beaufort D, Patrier P, Petit S (2002) Crystal Chemistry of Fe-sudoites from Uranium Deposts in the Athabasca Basin (Saskatchewan, Canada). Clays and Clay Minerals 50: 70-81.
2. Petit S, Decarreau A, Martin F, Buchet R (2004) Refined relationship between the position of the fundamental OH stretching and the first overtones for clays. Physics and Chemistry of Minerals 31: 585-592.
3. Vingiani S, Righi O, Petit S, Terribile F (2004) Mixed-layer kaolinite-smectite minerals in a red-black soil sequence from basalt in Sardinia (Italy). Clays and Clay Minerals 52: 473-483.
4. Carrado KA, Decarreau A, Petit S, Bergaya F, Lagaly G (2006) Synthetic clay minerals and purification of natural clays. Developments in clay science 1: 115-139.
5. Kodama H, Schnitzer M (1980) Effect of fulvic acid on the crystallization of aluminum hydroxides. Geoderma 24: 195-205.
6. Petit S, Righi D, Madejová J, Decarreau A (1998) Layer charge estimation of smectites using infrared spectroscopy. Clay Minerals 33: 579-591.
7. Rosenberg PE, Hooper RL (1996) Determination of the chemical composition of natural illites by analytical electron microscopy. Clays and Clay Minerals 44: 569-572.
8. Vogels RJMJ, Kloprogge JT, Geus JW (2005) Synthesis and characterization of saponite clays. American Mineralogist 90: 931-944.
9. Elfil H, Srasra E, Dogguy M (1995) Caracterisation physico-chimique de certaines argiles utilisees dans l'industrie ceramique. Journal of Thermal Analysis and Calorimetry 44: 663-683.
10. Schroeder PA, Pruett RJ, Hurst VJ (1998) Effects of secondary iron phases on kaolinite 27Al MAS NMR spectra. Clays and Clay Minerals 46: 429-435.
11. Castelein O, Aldon L, Olivier-Fourcade J, Jumas JC, Bonnet JP, et al. (2002) 57 Fe Mössbauer study of iron distribution in a kaolin raw material: influence of the temperature and the heating rate. Journal of the European Ceramic Society 22: 1767-1773.
12. Saikia NJ, Bharali DJ, Sengupta P, Bordoloi D, Goswamee RL, et al. (2003) Characterization, beneficiation and utilization of a kaolinite clay from Assam, India. Applied Clay Science 24: 93-103.
13. Maritan L, Nodari L, Mazzoli C, Milano A, Russo U (2006) Influence of firing conditions on ceramic products: experimental study on clay rich in organic matter. Applied Clay Science 31: 1-15.
14. Chandrasekhar S, Ramaswamy S (2007) Investigation on a gray kaolin from south east India. Applied Clay Science 37: 32-46.
15. Nodari L, Marcuz E, Maritan L, Mazzoli C, Russo U (2007) Hematite nucleation and growth in the firing of carbonate-rich clay for pottery production. Journal of the European Ceramic Society 27: 4665-4673.
16. Lecomte-Nana GL, Lesueur E, Bonnet JP, Lecomte G (2009) Characterization of a lateritic geomaterial and its elaboration through a chemical route. Construction and Building Materials 23: 1126-1132.
17. Cases JM, Lietard O, Yvon J, Delon JF (1982) Etude des propriétés cristallochimiques, morphologiques, superficielles de kaolinites désordonnées. Bulletin de Minéralogie 105: 439-457.
18. Lecomte-Nana G, Goure-Doubi H, Smith A, Wattiaux A, Lecomte G (2012) Effect of iron phase on the strengthening of lateritic-based "geomimetic" materials. Applied Clay Science 70: 14-21.
19. Alvarez-Puebla RA, Valenzuela-Calahorro C, Garrido JJ (2006) Theoretical study on fulvic acid structure, conformation and aggregation: a molecular modelling approach. Science of the Total Environment 358: 243-254.
20. Boustingorry P (2002) Elaboration d'un matériau composite à matrice gypse et renfort bois fragmenté. Amélioration de la résistance au vissage de produits préfabriqués en gypse (Doctoral dissertation, Ecole Nationale Supérieure des Mines de Saint-Etienne).
21. Rojas MF, Cabrera J (2002) The effect of temperature on the hydration rate and stability of the hydration phases of metakaolin–lime–water systems. Cement and Concrete Research 32: 133-138.
22. Schwertmann UT, Fischer WR (1973) Natural "amorphous" ferric hydroxide. Geoderma 10: 237-247.

23. Bhosale DN, Patil VY, Rane KS, Mahajan RR, Bakare PP, et al. (1998) Thermal study of ferritization temperature of Cu–Mg–Zn ferrites: TG/DTG/DTA (STA) studies. Thermochimica Acta 316: 159-165.

24. Soubrand-Colin M (2004) Localisation, distribution et mobilité des ETM dans des sols développés sur roches basaltiques en climat tempéré (Doctoral dissertation, Limoges).

25. Martin F, Ferrage E, Petit S, de PARSEVAL P, Delmotte L, et al. (2006) Fine-probing the crystal-chemistry of talc by MAS-NMR spectroscopy. European Journal of Mineralogy 18: 641-651.

26. Ortiz De Serra MI, Schnitzer M (1973) The chemistry of humic and fulvic acids extracted from argentine soils-I. Analytical characteristics. Soil Biology and Biochemistry 5: 281-286.

27. Schnitzer M, Kerndorff H (1981) Reactions of fulvic acid with metal ions. Water, Air, and Soil Pollution 15: 97-108.

28. Malomo S (1986) Penetration resistance and basic engineering properties of laterite profile soils. In Proceedings of the 5th International Congress of the International Association of Engineering Geology, Buenos Aires 2: 821-828.

29. Kovda IV, Morgun EG, Tessier D, Pernes M (2000) Particle orientation in clayey soils according to transmission diffractometry data. Pochvovedenie 8: 989-1003.

30. Djangang CN, Kamseu E, Ndikontar MK, Nana GLL, Soro J, et al. (2011) Sintering behaviour of porous ceramic kaolin–corundum composites: Phase evolution and densification. Materials Science and Engineering: A 528: 8311-8318.

31. Goodary R, Lecomte-Nana GL, Petit C, Smith DS (2012) Investigation of the strength development in cement-stabilised soils of volcanic origin. Construction and Building Materials 28: 592-598.

32. Goure-Doubi H, Martias C, Lecomte-Nana GL, Nait-Ali B, Smith A, et al. (2014) Interfacial reactions between humic-like substances and lateritic clay: Application to the preparation of “geomimetic” materials. Journal of Colloid and Interface Science 434: 208-217.

33. MacCarthy P, Perdue EM (1991) Complexation of metal ions by humic substances: fundamental considerations. In Interactions at the Soil Colloid—Soil Solution Interface (pp: 469-489). Springer Netherlands.

34. Schnitzer M, Kodama H (1992) Interactions between organic and inorganic components in particle-size fractions separated from four soils. Soil Science Society of America Journal 56: 1099-1105.

35. Malomo S (1982) Use of the word 'laterite' in engineering geology - A review pp: 201-208.

36. Houston JR, Herberg JL, Maxwell RS, Carroll SA (2008) Association of dissolved aluminum with silica: Connecting molecular structure to surface reactivity using NMR. Geochimica et Cosmochimica Acta 72: 3326-3337.